

Preliminary results for mask metrology using spatial heterodyne interferometry

Philip R. Bingham^{1 a}, Kenneth W. Tobin^a, Marylyn H. Bennett^b and Pat Marmillion^b

^aOak Ridge National Laboratory², Oak Ridge, Tennessee, 37831-6010

^bInternational SEMATECH, Austin, Texas, 78741-6499

ABSTRACT

Spatial heterodyne interferometry (SHI) is an imaging technique that captures both the phase and amplitude of a complex wavefront in a single high-speed image. This technology was developed at the Oak Ridge National Laboratory (ORNL) and is currently being implemented for semiconductor wafer inspection by nLine Corporation. As with any system that measures phase, metrology and inspection of surface structures is possible by capturing a wavefront reflected from the surface. The interpretation of surface structure heights for metrology applications can become very difficult with the many layers of various materials used on semiconductor wafers, so inspection (defect detection) has been the primary focus for semiconductor wafers. However, masks used for photolithography typically only contain a couple well-defined materials opening the doors to high-speed mask metrology in 3 dimensions in addition to inspection. Phase shift masks often contain structures etched out of the transparent substrate material for phase shifting. While these structures are difficult to inspect using only intensity, the phase and amplitude images captured with SHI can produce very good resolution of these structures. The phase images also provide depth information that is crucial for these phase shift regions. Preliminary testing has been performed to determine the feasibility of SHI for high-speed non-contact mask metrology using a prototype SHI system with 532nm wavelength illumination named the Visible Alpha Tool (VAT). These results show that prototype SHI system is capable of performing critical dimension measurements on 400nm lines with a repeatability of 1.4 nm and line height measurements with a repeatability of 0.26nm. Additionally initial imaging of an alternating aperture phase shift mask has shown the ability of SHI to discriminate between typical phase shift heights.

Keywords: Mask Inspection, Mask Metrology, Spatial Heterodyne Interferometry

1. INTRODUCTION

The ability to perform accurate mask metrology is a requirement of lithographic technology for the control of mask patterning processes. At the 130nm technology node specified in the International Technology Roadmap for Semiconductors (ITRS), the minimum printed feature dimension on the wafer is 100nm with a corresponding minimum mask feature size of 100nm and 400nm for a 1X and 4X mask respectively. The ability to perform mask metrology in a cost-effective, high-throughput environment is becoming difficult to achieve with optical technology, even as microscopy systems reach into the deep ultra-violet (DUV) to achieve higher resolution. While scanning electron microscopy (SEM) systems provide the highest potential resolution for semiconductor metrology today, the high-cost, high-maintenance, and vacuum operating environment make them difficult to adapt to a low-cost, high-throughput mask measurement. The Oak Ridge National Laboratory (ORNL) has developed a digital holographic imaging technology using spatial heterodyne interferometry (SHI) with a demonstrated in-plane (x,y) resolution of close to $\lambda/4$ (using a patent-pending off-axis recombination method) and out-of-plane (z) resolution of $\lambda/100$, where λ

¹ P.R.B. (Correspondence): Email: binghampr@ornl.gov; WWW: <http://www-ismv.ic.ornl.gov>; Telephone: (865) 574-5680; Fax: (865) 576-8380.

² Prepared by the Oak Ridge National Laboratory, Oak Ridge, Tennessee, 37831-6285, operated by UT-Battelle, LLC for the U.S. Department of Energy under contract DE-AC05-00OR22725.

is the wavelength of the laser illumination source. A prototype tool has been developed by ORNL for nLine Corporation, Austin, Texas. Although this tool was originally developed for inspecting high-aspect ratio features such as contacts, vias, and trenches [1,2,3], the technology has the potential to perform optical, high-resolution structural metrology in a cost-effective mask metrology environment.

A study has been performed on the feasibility of performing mask metrology using the digital holographic imaging technology. ORNL has investigated the ability of the holographic imaging tool to perform reflective phase measurements on binary and phase shifting lithographic mask elements. From a measurement of optical phase (i.e., a measurement of the shift in the argument of a reference wavefront relative to a wafer that has been modulated by an inspected surface), a measurement of the surface height and or the characteristics of the surface materials (e.g., the index of refraction) can be made. Our goal with this effort has been to both qualify and quantify the ability of the non-contact SHI measurement technique to characterize mask surfaces and to make these measurements in an accurate and repeatable manner. As an introduction, the following sections describe the SHI imaging technology followed by an introduction to using SHI for mask metrology.

1.1. Spatial heterodyne interferometry system

Spatial heterodyne interferometry (SHI) is an imaging technique that captures both the phase and amplitude of a complex wavefront in a single high-speed image. This technique closely resembles phase shifting interferometry, in that two wavefronts are interfered with one another on the surface of an imaging sensor; however, in SHI the two beams are interfered at a small angle with respect to one another to spatially heterodyne the complex wavefront. This allows SHI to reconstruct phase with only a single image whereas phase shift interferometry requires multiple images. Thus, the SHI technique provides a phase measurement suitable for high-speed metrology/inspection.

Figure 1 shows the basic system design for SHI used in the prototype at ORNL named the Visible Alpha Tool (VAT). In the VAT, the illumination is provided by a 532nm CW laser. A beam splitter divides the beam into a target and a reference beam. The target beam follows a path that strikes the surface to be measured (the mask in this case) before traveling on to the camera while the reference beam follows an identical path with the test object replaced by a flat mirror. Acousto-Optic Modulators (AOMs) are used in both the reference and target arms of the system to shutter the illumination and provide power balancing between the two beams. The final beam splitter before the camera is rotated to set up the desired angle between the reference and target arms.

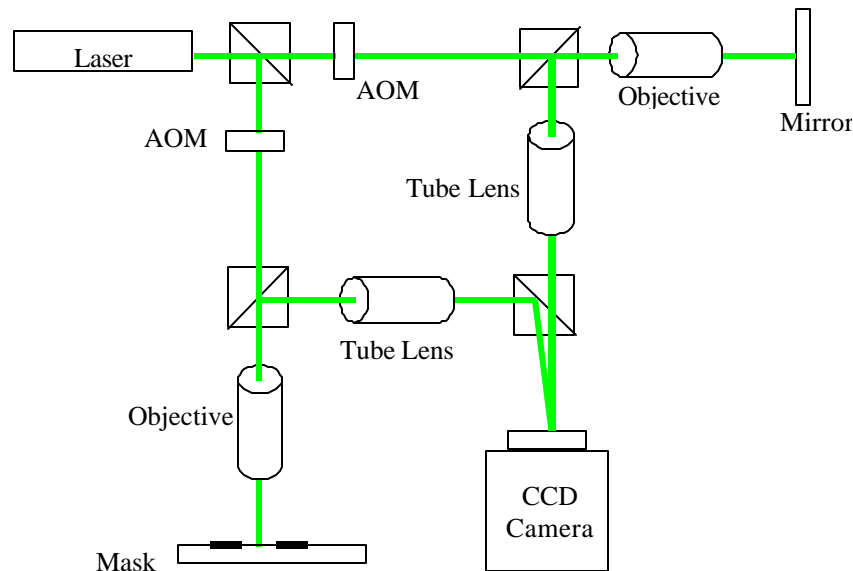


Figure 1. Basic SHI system layout.

The image capture rate for the VAT is limited to 30 frames (1024x1024 pixels x 12 bit) per second by the camera, but reconstruction of the acquired image to obtain the phase and amplitude images limits the

prototype to 3 frames per second. Parallelism associated with reconstructing multiple images allows the reconstruction process to be easily sped up with parallel processing. The VAT resolution is approximately 266nm, since 532nm coherent illumination is being used, in the plane of the object surface with 5 to 10nm resolution measured on the prototype in the direction normal to the surface.

1.2. SHI image reconstruction

The process of hologram image formation can be adequately described using scalar diffraction theory [4], where the reference wavefront, $U_o(x,y)$ and the reflected wavefront, $U_R(x,y)$, are described as,

$$U_o(x, y) = A_o(x, y) e^{-ij(x,y)} \quad \text{and} \quad U_R(x, y) = A_R(x, y) e^{-jy(x,y)} .$$

The intensity of the sum of these two wavefronts, $I(x,y)$, is recorded, e.g., on a photographic film media or in our case directly on the surface of a CCD camera, and is expressed as,

$$I(x, y) = |A_o(x, y)|^2 + |A_R(x, y)|^2 + 2 A_o(x, y) A_R(x, y) \cos(\mathbf{y}(x, y) - \mathbf{f}(x, y)) ,$$

which contains information not only regarding the intensity of the two waves, but also the relative phase between them at every spatial location (x,y) .

The ORNL method uses a reference wavefront that is planar and therefore we can replace this value in the above equations with $U_o(x,y) = I$. Also, the system has been designed to form uniform, linear fringes in the intensity plane that are modulated by the surface topology and the indices of refraction of the various materials composing the surface. Taking this into account, the hologram equation can be rearranged and more succinctly expressed as,

$$I(x, y) = 1 + |A_R(x, y)|^2 + 2 \mathbf{m} A_R(x, y) \cos[2\mathbf{p}(\mathbf{w}_x x + \mathbf{w}_y y) + \mathbf{f}(x, y)] ,$$

where \mathbf{m} is measure of coherence between the two wavefronts that affects fringe contrast, and \mathbf{w}_x and \mathbf{w}_y are constant frequency components of the cosine function. The frequency constants, $(\mathbf{w}_x, \mathbf{w}_y)$, represent the carrier frequency of the system and facilitate a recovery of the amplitude, $A_R(x,y)$ and the phase, $\mathbf{f}(x,y)$, by using a Fourier frequency analysis. Figure 2 shows an example of the intensity hologram formed on a CCD sensor for a chrome-on-glass target. The inset in Figure 2 is an enlarged region showing the linear sinusoidal fringe pattern that is being modulated by the surface topology and material characteristics.

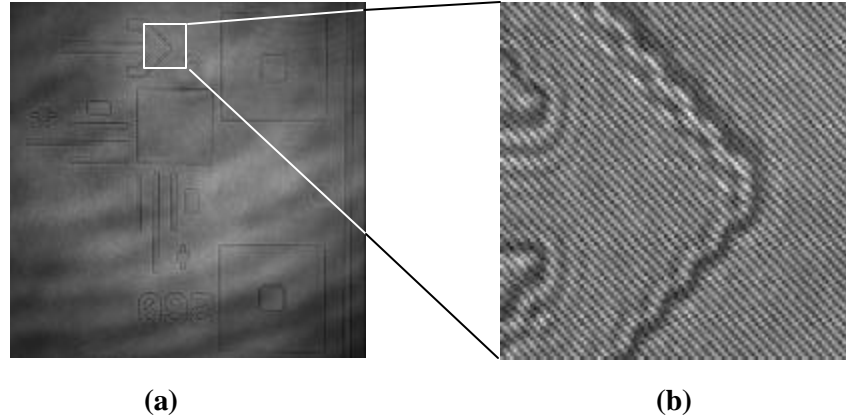


Figure 2. Example in (a) of a recorded hologram of a chrome-on-glass target. The inset in (b) shows the linear sinusoid patterns of fringes represented by (w_x, w_y) that is being modulated by the surface structure, which is a function of the phase, $f(x,y)$.

The result of the Fourier frequency analysis is the approximate determination of the original complex wavefront, i.e.,

$$U_F(x, y) = 2 \mathbf{m} A_R(x, y) e^{-j\mathbf{f}(x,y)} \approx U_R(x, y)$$

Once an estimate of the original complex wavefront, $U_F(x,y)$, has been determined, the amplitude and phase are determined by,

$$A_R(x,y) = \sqrt{\text{Re}\{U_F(x,y)\}^2 + \text{Im}\{U_F(x,y)\}^2} \quad \text{and} \quad f(x,y) = \tan^{-1}\left(\frac{\text{Re}\{U_F(x,y)\}}{\text{Im}\{U_F(x,y)\}}\right),$$

where $\text{Re}\{\}$ and $\text{Im}\{\}$ represent the real and imaginary components of $U_F(x,y)$ respectively. Figure 3 shows the resultant amplitude of the chrome-on-chrome target in (a) and the phase reconstruction of a portion of the target in (b).

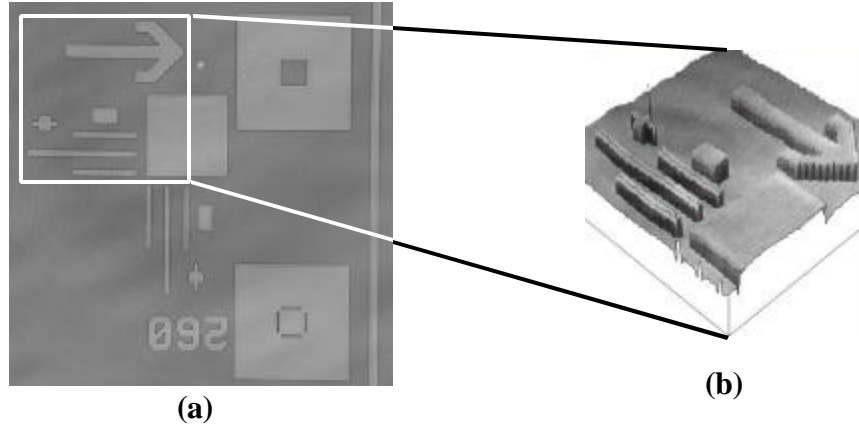


Figure 3. Resulting amplitude, $A_R(x,y)$, in (a) and phase, $f(x,y)$ in (b) of the chrome-on-chrome target shown in Figure 2.

1.3. Mask Metrology

While SHI has been demonstrated to perform well for detecting defects in high-aspect ratio structures on patterned wafers [1,2,3], our goal through this study was to demonstrate the ability to apply this technology to a metrology application for mask characterization. In defect inspection the main emphasis is on the detection of missing or extra materials on the wafer surface. Therefore, the method used to identify the presence of unexpected structure or contamination is to compare like-regions on the wafer to each other by the well-known method of die-to-die comparisons. While the magnitude of the anomaly on the wafer surface is of importance, the driving principle in the development of the inspection tool is sensitivity, i.e., to produce a tool that can detect critical anomalies of a sufficiently small size while accommodating normal or expected process variability in a die-to-die comparison.

For mask metrology the goal is different. The goal is to make a determination of the absolute width and depth of printed lines, determine the roughness or shape of these lines, and perhaps most importantly, to measure the phase shifting properties of the mask that result either from the removal of material from the transparent regions of the mask or from the addition of phase-shifting materials to the surface of the mask. The SHI method is well suited to make robust and repeatable measurements of surface structure and phase shifting materials in a manner that has advantages over common techniques used today such as incoherent optical microscopy and scanning electron microscopy.

Figure 4 shows schematically several of the challenges and advantages that can be achieved by making mask measurements using SHI. In the figure, a reference wave, $U_o(x,y)$ is shown impinging on the surface of the mask. This wave is reflected, $U_R(x,y)$, from the mask surfaces and the surface topology and material properties cause a modulation of the wavefront that is encapsulated in the amplitude, $A_R(x,y)$ and the phase, $f_R(x,y)$ of the reflected wavefront. The amplitude mainly contains information on the reflectivity of the various surfaces of the mask.

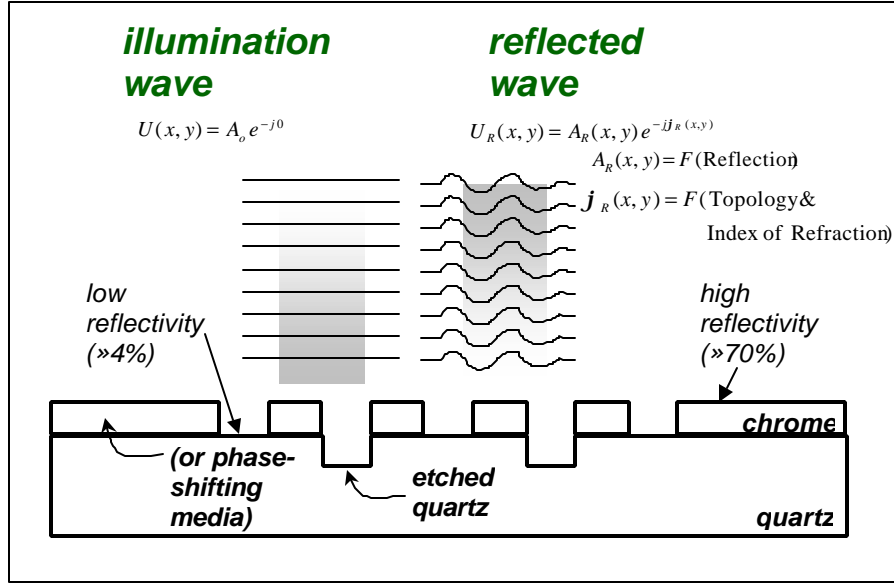


Figure 4. Schematic of wavefront reflection from lithographic mask highlighting challenges for inspection with SHI.

The first challenge is the dynamic range required to image binary masks. On a binary mask, the reflectivity of the opaque regions is much higher than the reflectivity of the substrate. This high contrast allows the conventional optical microscope to discriminate between these two regions, but for SHI the contrast modulates the fringes. Therefore, the camera must have enough dynamic range such that the fringe pattern is distinguishable in both the chrome areas (not bloomed out) and the quartz areas (not under exposed). A majority of the mask metrology testing to date has been performed with binary masks, and the results have shown that the dynamic range of our prototype system is suitable for mask metrology.

The second challenge is whether the phase information captured can be interpreted to obtain metrology information since it is a combination of both topology and the complex index of refraction for the materials. For a uniform material, conversion of the reflected phase measurements to structure heights is calculated by $\Delta Z = l(q_2 - q_1) / 4p$; however, when a wave reflects off of the surface of a material, a phase shift dependent on the complex index of refraction occurs. In many transparent materials, or dielectrics in general, the imaginary component of the complex index of refraction is negligible. For opaque materials like chrome, the imaginary component can be significant. Therefore, the reflection phase shift will vary between materials. This reflection phase shift must be included in the height calculation to properly measure the true height change between materials. Using the Fresnel equations and assuming the illumination angle of incidence is near normal, the height difference between two materials with different indices of refraction given the measured phase (i.e., q_1 and q_2) on each of the two materials is given by [5],

$$\Delta Z = \frac{l}{4p} \left[(q_2 - q_1) - \left(\tan^{-1} \left[\frac{2k_2}{n_2^2 + k_2^2 - 1} \right] - \tan^{-1} \left[\frac{2k_1}{n_1^2 + k_1^2 - 1} \right] \right) \right]$$

The index of refraction for each material is defined as $N_i = n_i + jk_i$. This is particularly important for mask metrology, because as mentioned above, chromium has a significant k component and quartz does not have a k component. Thus, the measured phase height between chrome and quartz will be smaller than the same phase height measured over a uniform material with the same topology. Since the typical mask consists of only two materials, these calculations remain fairly simple and surface metrology of masks is feasible.

If the high contrast of a binary mask allows a traditional optical microscopy system to discriminate between the chrome and quartz regions of a mask, why use SHI for mask metrology? In other words, what are the

advantages of SHI over traditional optical metrology? There are several reasons to use SHI over traditional optical microscopy. Two key reasons are phase region discrimination and surface metrology.

SHI has the ability to discriminate between phase shift regions of a mask. Masks are quickly changing from binary to various types of phase shifting schemes. In an alternating phase shift mask (PSM), the quartz is etched down to produce phase shifts in the light passing through the mask. These etched areas are typically at two levels to produce 0 and 180 degree shifts with the possibility of including 60 and 120 degree shifts for improved resolution. As these etched areas are all in the mask substrate, the reflectivity is the same for all shift regions. Thus, the optical microscope would be unable to discriminate between these various phase shift regions. However, the height difference between these shifting areas will appear in the phase portion of the SHI measurement allowing discrimination between these areas.

SHI provides measurements in the direction normal to the surface. For mask metrology, this surface height measurement capability allows SHI to determine whether a phase shifting area is the proper height required to produce the desired phase shift. In general, this allows SHI to monitor the surface quality of both the blocking layer and the substrate layer of a mask. While other systems such as atomic force microscopes (AFMs) are capable of providing precise surface topology measurements, the SHI system provides a surface topology measurement at a very high speed over a large area. Figure 5 shows a phase image of a binary mask taken during testing along with the inset of an AFM scan performed over the small area outlined in the image. The SHI data was collected over approximately 1/30th of a second and reconstructed into the phase image shown in less than 1/2 second, whereas the AFM data took many minutes to collect. The line scan at the bottom of the phase image corresponds to the line across the image.

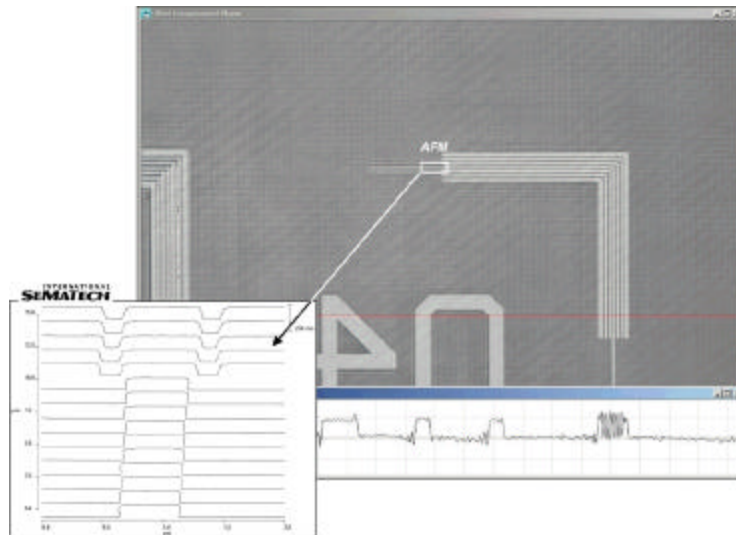


Figure 5. Example of a 400nm line region measurement made using the VAT. The image at lower left shows a set of line measurements made on a single 400nm structure by CD AFM.

2. PRECISION TESTING

Measurement precision can be divided into repeatability and reproducibility of the tool performance [6]. Repeatability is a measure of the performance of repeated measurements over a short time with no changes to the overall system between measurements. Reproducibility is a measure of performance over a longer period with changes made to the measurement system between measurements (e.g., the removal and replacement of a mask in the tool over a number of days). In this study, a series of tests have been performed to determine the repeatability of both critical dimension (CD) and line height measurements on the VAT. The VAT was developed as a wafer inspection tool and therefore does not currently have algorithms specific to alignment and auto-focus on masks. For this reason, the reproducibility results are

not useful and are not presented in this work. Although no standards were available for relative height accuracy testing, line height measurements were compared with measurements acquired on an AFM by International SEMATECH.

2.1. Test methodology

Since SHI provides information in three dimensions, experiments were developed to measure the line width for testing of in-plane variations and phase height of the lines for out of plane (height) variations. Due to availability, a binary mask with test structures of various sizes was used for this study. Repeatability for width and height were measured by performing 100 measurements at three locations along a line in the 1000nm and 400nm test structures. The left side of Figure 6 graphically shows a top down view of a line end with the measurement locations. Measurements were made on dense lines of the 1000nm structure and isolated lines of the 400nm structure. An isolated line was used for the 400nm structure since sampling was marginal and line interference was prevalent in the dense line regions. Figure 7 provides images of the two structures and the location of measurements in the structure for the 1000nm dense lines (left) and 400nm isolated lines (right). The right side of Figure 6 shows width measurements were made at 10%, 50%, and 90% of the phase height. The width measurements could also be performed in the intensity image; however, the phase image provides a much cleaner signal to work with due to diffraction at the line edges in the intensity images.

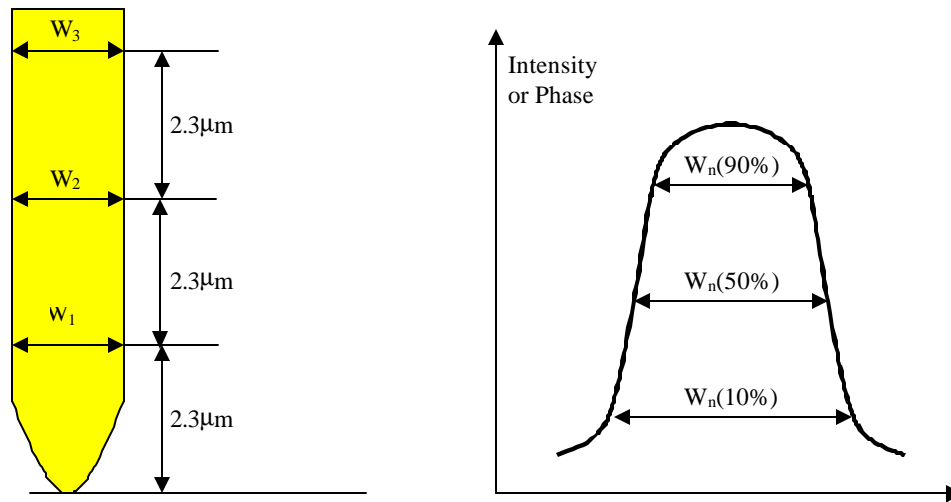


Figure 6. Schematic representation of measurement locations. Left image shows top-down view of multiple measurement positions along a line used to measure CD and heights, the right-hand image shows the positions along the height of the structure that were measured.

Since SHI provides surface topology information, not only was width (CD) obtained during testing, but height measurements were taken as well. Phase differences between the chrome and quartz at each measurement location were calculated as a measure of chrome height in degrees. For both the line width and height measurement sets, the mean and standard deviation for each measurement type and location were calculated using 100 samples per site to determine repeatability of the measurements.

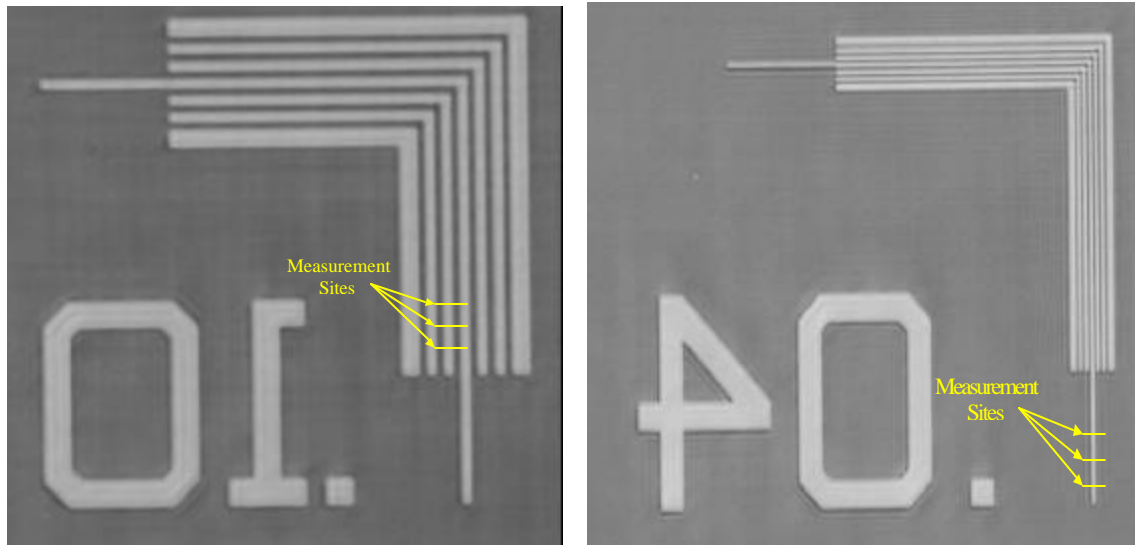


Figure 7. Measurement sites for the 1000nm dense line structure and 400nm for the isolated line structure.

A key component in precision of measurements from a metrology tool is extraction of the values of interest from the captured image. A very basic approach has been taken for this first application of the digital holographic method to metrology. For this feasibility study, calculations for width and height were made for a single line in the image. First a profile along a single line was extracted from the image to make the measurements. Figure 8 shows example profiles from both the 1000nm dense and 400nm isolated lines used in the testing.

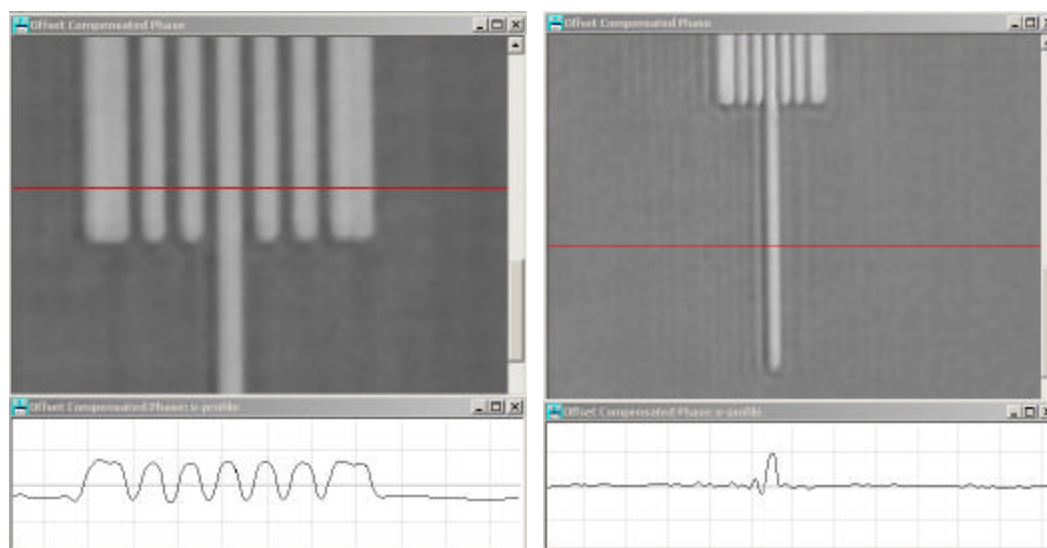


Figure 8. Profiles of 1000nm dense lines and 400nm isolated line.

In the 1000nm region, the third line/bump from the left was used for the test. Since the 1000nm lines are well above the resolution of the VAT, a smoothing filter could be used with no loss to the height of the lines. This produced the nice smooth profile for these lines, which in turn allows the top and bottom of the lines to be easily located in the profile. However, the 400nm lines are quickly approaching the resolution of the VAT and a smoothing filter begins to significantly degrade the line height and width. The 400nm line profile shows ringing on the left side of the lines. Ringing is due to diffraction, but the asymmetry of the ringing is likely due to aberrations in the optical system.

A method for extracting width and height was developed to handle both the 1000nm and 400nm profiles. In this method, the operator identifies the location of the line center as close as possible and identifies the design line width. Using the phase image, the algorithm performs a local maximum search in a region the size of one line width to find the top of the line. Next a search is performed to the right of the line for a local minimum within one line width of the peak. The minimum search is made to the right due to the reduced ringing in the right direction. The phase values at the minimum and maximum are subtracted to determine the phase height of the line.

Phase height at 10, 50, and 90% of the maximum are calculated and used to locate the 10, 50, and 90% width locations on each side of the line. These positions are located by searching out from the maximum until the phase value drops below the 10, 50, or 90% threshold. This is followed by a linear interpolation step used to obtain sub-pixel resolution.

2.2. Critical dimension and line height repeatability results

The repeatability tests were performed 5 times at each location over a number of days. Table 1 shows the results obtained from repeatability testing on the 1000nm dense lines. This table shows the results for all three measurement locations with the mean of the average and standard deviations for the 5 tests. The results for each of these tests show the mean values and standard deviations for 10, 50, and 90% line width in nanometers and the same values for height measurements in degrees. The VAT uses a 532nm laser; therefore, one degree of phase height corresponds to approximately 0.739nm. At the bottom of the table, average values for standard deviation are given for each of the four measurements. Width measurements have repeatability in the 10nm range and height measurements have average repeatability of 0.90 degrees (0.665nm).

Table 1 - Repeatability measurements for 1000nm dense lines. (100 samples per test)

Site	Width (nm)						Height (degrees)	
	10%		50%		90%		Mean	σ
	Mean	σ	Mean	σ	Mean	σ		
1	1541.15	9.94	1106.96	8.73	586.01	10.91	109.80	0.86
2	1563.65	8.97	1114.51	7.36	581.90	9.71	106.80	0.94
3	1551.47	11.24	1096.45	8.87	559.68	11.81	104.41	0.90
Average		10.05		8.32		10.81		0.90

Table 2 shows the repeatability results for the 400nm isolated line tests. Notice the height of the lines has dropped from the 105 degree range on the 1000nm lines to the 95 degree range for the 400nm lines. This is due to the 400nm lines approaching the resolution limits of the VAT. Average standard deviations shown at the bottom of the table indicate that the repeatability for isolated 400nm lines is 12.4nm for 10% width, 6.7nm for 50% width, 7.7nm for 90% width, and 1.75degrees (1.29nm) for height.

Table 2 - Repeatability measurements for 400nm isolated lines. (100 samples per test)

Site	Width (nm)						Height (degrees)	
	10%		50%		90%		Mean	σ
	Mean	σ	Mean	σ	Mean	σ		
1	746.60	15.88	488.23	7.40	216.16	7.15	93.46	2.04
2	746.74	11.39	496.89	5.65	217.83	7.74	91.06	1.79
3	743.90	9.97	497.82	6.90	221.77	8.33	97.30	1.44
Average	745.75	12.41	494.31	6.65	218.59	7.74	93.94	1.76

The repeatability measurements shown in the previous tables provide results that correspond to making a measurement with a single sample. Oversampling will improve the precision of the results and this

improvement is typically calculated as, $E_{Oversampled} = E / \sqrt{\text{Number Of Samples}}$. Standard deviations were calculated for each measurement with averaging of 1, 4, 10, and 25. Repeatability of the VAT measurements with oversampling are tabulated in Table 3 for 1000nm dense lines and Table 4 for 400nm

isolated lines. Sampling 25 times for each measurement reduces the repeatability error to approximately 2nm for all width measurement on both line widths. Repeatability error reduces to 0.18 degrees (0.133nm) for 1000nm lines and 0.35 degrees (0.259nm) for the 400nm lines. Note that the time required to collect 25 repeated measurements on the VAT is a approximately 25 x 1/30th sec, i.e., less than 1 sec. Reconstruction of 25 measurements takes approximately 8 seconds; however, due to the highly parallel nature of this problem, the reconstruction time can be easily reduce, and nLine has already accomplished this speed increase with their semiconductor wafer inspection system.

Table 3 - Repeatability results for 1000nm dense lines with oversampling.

Samples	Width σ (nm)			Height σ (degrees)
	10%	50%	90%	
1	10.05	8.32	10.81	0.90
4	5.03	4.16	5.41	0.45
10	3.18	2.63	3.42	0.28
25	2.01	1.66	2.16	0.18

Table 4 - Repeatability results for 400nm dense lines with oversampling.

Samples	Width σ (nm)			Height σ (degrees)
	10%	50%	90%	
1	12.41	6.65	7.74	1.75
4	6.21	3.33	3.87	0.88
10	3.92	2.10	2.45	0.55
25	2.48	1.33	1.55	0.35

2.3. Relative height accuracy

As a final characterization of the VAT performance for mask metrology, the accuracy of the height measurements are reported relative to height measurements made on the same mask in the same regions with the CD AFM at ISMT. The AFM measurements show that the chrome height on this mask is 99.1nm \pm 1.0nm. As shown earlier, the height calculation requires consideration of the complex indices of refraction. While we do not know the composition of the chrome on this mask, a good approximation would be to use the index for chromium. The index of refraction for chromium at a wavelength of 532nm is 2.9+j4.44, and the index of refraction for quartz is 1.55 at 532nm [7].

The average phase difference between the quartz and chrome in the precision testing in the region near where the CD AFM scan was performed is 109.8 degrees (0.61 π radians). Thus we can calculate the measured chrome height as,

$$\begin{aligned} \Delta Z &= \frac{I}{4p} \left[(0.61p) - \left(\tan^{-1} \left[\frac{2 \cdot 0}{1.55^2 + 0^2 - 1} \right] - \tan^{-1} \left[\frac{2 \cdot 4.44}{2.9^2 + 4.44^2 - 1} \right] \right) \right] \\ &= \frac{I}{4p} [0.61p + 0.3164] = 94.5\text{nm}. \end{aligned}$$

This value is 4.6nm lower than the AFM value. While we have taken into consideration the material difference on the first order in our calculation, several other items will affect the phase measurement obtained from reflection such as oxide and polish layers that may be present on the surface. Reference [5] lists several of these items and provides equations for handling them. In an example within this paper, a 5nm oxide layer is assumed to be on the surface of both the chrome and glass surfaces of a measurement standard. This layer would not show a height difference between the chrome and quartz for a contact profilometer, but would alter the phase values obtained from a reflected interferometry measurement. In the example, this 5nm oxide layer reduced the perceived height by 5nm. Therefore, an oxide layer could easily account for the 4.6nm difference between the digital holography measurement and the AFM measurement. Another possible source of error is the assumption that the index of refraction for chromium can be used for the chrome layer of the test mask, whose precise material composition was unknown.

2.4. Phase shift mask metrology

During this study, tests were not performed to determine the ability of this tool to make measurements on phase shifting regions of a phase shifting mask. As discussed previously, this measurement of height difference between two phase shifting regions on an alternating aperture phase shift mask is more direct in that the index of refraction can be ignored, because measurements are being taken between different heights of the same material. Images have been captured on the 532nm VAT of an alternating aperture phase shift mask designed for 248 nm illumination. Figure 9 shows a phase image taken from one area on the mask. The chrome lines in the image are approximately 520 nm wide with a 2:1 pitch. This figure shows that the VAT tool is able to easily distinguish between the two different phase shifting regions as expected.

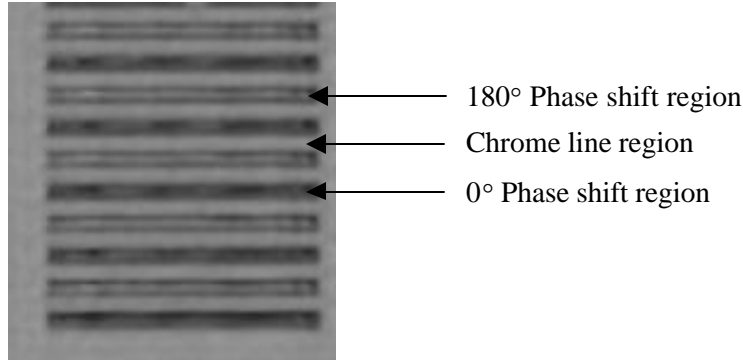


Figure 9. Phase image of 248nm AAPSM.

Table 5 shows expected phase responses from SHI systems with varying illumination on both 248nm and 193nm masks. This table was calculated assuming a quartz index of refraction of 1.55 for all wavelengths. For more precise calculation, the index of refraction for the various wavelengths is needed for the particular substrate material. While phase measurements do provide a surface height measurement, phase wrapping does occur such that two levels with phase height differences 360 degrees apart appear the same unless unwrapping is possible. For phase shift masks with discrete levels, unwrapping is not possible. Phase shifting masks commonly use phase shift regions of 0 and 180 degrees and can include 60 and 120 regions. These discrete phase levels make metrology with phase measurement more feasible since these levels are likely to produce different phase results even in the presence of wrapping.

Table 5. Etch Depths and SHI responses for 248 and 196nm phase shift masks.

Phase Shift	0°	60°	120°	180°
248 nm Mask				
Etch Depth (nm)	0	75.2	150.3	225.5
Measurement Wavelength (nm)	Phase Measurement			
532	0°	101.7°	203.4°	305.1°
248	0°	218.2°	436.4°(76.4°)	654.5°(294.5°)
193	0°	280.4°	560.7°(200.7°)	841.1°(121.1°)
193 nm Mask				
Etch Depth (nm)	0	58.5	117.0	175.5
Measurement Wavelength (nm)	Phase Measurement			
532	0°	79.2°	158.3°	237.5°
248	0°	169.8°	339.6°	509.4°(149.4°)
193	0°	218.2°	436.4°(76.4°)	654.5°(294.5°)

Table 5 provides an understanding of the phase height measurements from the most common phase shifting levels depending on the wavelength of the mask and the wavelength of the inspection illumination. Notice the wraps will require a metrology tool to take the illumination and inspection wavelengths into consideration when trying to distinguish between phase shifting regions.

3. CONCLUSIONS

ORNL has completed a series of measurements on a binary mask that demonstrate the feasibility of using the digital holographic microscopy method for mask metrology. This includes qualitative measurements that demonstrate the high-speed, wide-area imaging capabilities of the VAT (i.e., relative to the individual line scans that must be collected using a CD AFM). Regardless of the fact that the VAT system was originally designed for wafer inspection - quantitative line width (i.e., CD) measurements resulted in repeatability precisions of approximately 2nm for both the 400nm and 1000nm line widths. Line heights were repeatable to 0.133nm for the 1000nm lines, and 0.259nm for the 400nm lines. These measurements used 25 repeated measurements at each site on the mask. Relative accuracy measurement for line height measurements was investigated. Height measurements of 94.5nm were made with the VAT as compared to the AFM tool measurement of $99.1\text{nm} \pm 1.0\text{nm}$. This difference was well within the unknown characteristics of the material compositions and potential oxide coatings that may have existed on the surface of the mask.

In summary, there were no apparent limitations identified that would reduce the applicability of this technology to the measurement and characterization of lithographic masks. Continued work in this area will include investigation of the potential of the method to perform metrology and inspection for phase shifting masks.

ACKNOWLEDGEMENTS

We would like to thank nLine Corporation for use of the VAT for in performing this research. Likewise, we would like to thank International SEMATECH for funding, for test masks, and for AFM scans that Ron Dixon provided for comparison.

REFERENCES

-
- [1] C.E. Thomas, et al., "Direct to Digital Holography for Semiconductor Wafer Defect Detection and Review", Design, Process Integration, and Diagnostics in IC Manufacturing, Proceedings of the SPIE Vol. 4692, March 2002.
- [2] M. A. Schulze, M. A. Hunt, E. Voelkl, J. D. Hickson, W. R. Usry, R. G. Smith, R. Bryant, and C. E. Thomas, Jr., "Semiconductor wafer defect detection using digital holography", Design, Process Integration, and Diagnostics in IC Manufacturing, February 2003.
- [3] Thomas, C.E., et al., "Direct to Digital Holography for High Aspect Ratio Inspection of Semiconductor Wafers," 2003 International Conference on Characterization and Metrology for ULSI Technology, March 24-28, 2003.
- [4] J.W. Goodman, Introduction to Fourier Optics, McGraw-Hill Physical and Quantum Electronics Series, McGraw-Hill Book Co., New York, New York, 1968.
- [5] E.L. Church and S.R. Lange, "Structure Effects in Optical Surface Metrology," SPIE Vol. 680, Surface Characterization and Testing (1986), pp. 124-130.
- [6] Handbook of Silicon Semiconductor Metrology, Alain Diebold, Editor, Marcel Dekker, Inc., New York, New York, 2001.
- [7] CRC Handbook of Chemistry and Physics, 67th Edition, 1986-87, pp. E377-E392.